colorants

MDPI

Article

Long-Alkyl Chain Functionalized Imidazo[1,5-*a*]pyridine Derivatives as Blue Emissive Dyes

Gioele Colombo [1], Anita Cinco [1,2], G. Attilio Ardizzoia [1] and Stefano Brenna [1,*]

[1] Dipartimento di Scienza e Alta Tecnologia, Università degli Studi dell'Insubria and CIRCC, Via Valleggio 9, 22100 Como, Italy
[2] Scuola di Dottorato PhD-SDC, Scuola Universitaria Superiore IUSS Pavia, Palazzo del Broletto, Piazza Vittoria 15, 27100 Pavia, Italy
* Correspondence: stefano.brenna@uninsubria.it

Abstract: A series of boron difluoride compounds with 2-(imidazo[1,5-*a*]pyridin-3-yl)phenols bearing alkylic chains at the 1-position has been synthesized and characterized both with ^{1}H and ^{13}C NMR and infrared spectroscopy. This series of compounds displayed blue emission in solution and in thin polymeric films, with interesting features like large Stokes shifts and good fluorescence quantum yields. Time-Dependent Density Functional Theory (TD-DFT) calculations allowed for the identification of the main electronic transitions as intra ligand transitions (^{1}ILT), as corroborated by the Natural Transition Orbitals (NTOs) shapes.

Keywords: boron difluoride; imidazo[1,5-*a*]pyridine; blue emission; fluorescence; TD-DFT

Citation: Colombo, G.; Cinco, A.; Ardizzoia, G.A.; Brenna, S. Long-Alkyl Chain Functionalized Imidazo[1,5-*a*]pyridine Derivatives as Blue Emissive Dyes. *Colorants* **2023**, *2*, 179–193. https://doi.org/10.3390/colorants2020012

Academic Editors: Nadia Barbero, Carlotta Pontremoli and Simone Galliano

Received: 13 February 2023
Revised: 6 March 2023
Accepted: 3 April 2023
Published: 10 April 2023

1. Introduction

Imidazo[1,5-*a*]pyridines are heterocyclic compounds widely known in the literature due to their use in the fabrication of optoelectronic devices or as ligands in the synthesis of many coordination compounds [1,2]. They also displayed a wide range of different biological activities, such as antitumoral [3,4] and antibacterial effects [5,6], and for the treatment of Alzheimer's disease [7]. These compounds are also well known for their luminescence properties; in fact, they have been used as probes even in living cells, towards several analytes, such as Hg^{2+} [8], H_2S [9] and sulfites [10]. Moreover, it has been recently reported by Zhang that a coordination polymer derived from imidazo[1,5-*a*]pyridine is capable of detecting Cu^{2+}, CrO_4^{2-} and $Cr_2O_7^{2-}$ ions in water solution [11]. Even more studied is the ability of imidazo[1,5-*a*]pyridines to act as ligands with a large variety of metal centers. This allows us to obtain luminescent coordination compounds that can, in principle, be used in the fabrication of optoelectronic devices, such as Organic Light Emitting Diodes (OLEDs). These ligands, depending on the substituent on the main core, can bind the coordination center in various ways, starting from bidentate ligands [12], to tridentate [13] and even tetradentate [14] (Figure 1).

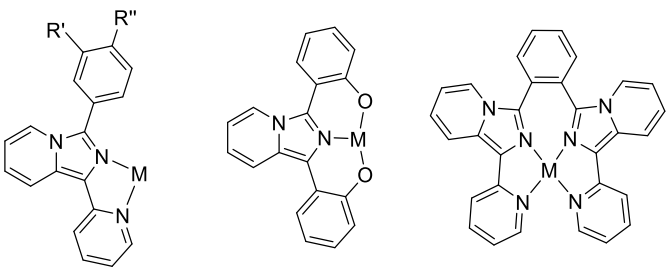

Figure 1. Three examples of different binding modes displayed by imidazo[1,5-*a*]pyridine derivatives: bidentate (Ref. [12]), tridentate (Ref. [13]) and tetradentate (Ref. [14]).

One of the most common substituent on the main core is the pyridinyl ring on the position 1: this permits a typical *N*,*N* bidentate coordination mode, which can be suitable for binding to many transition metal ions, such as Mn^{2+}, Ir^{3+}, Cu^{+}, Ag^{+}, Zn^{2+}, Ru^{2+} and Os^{2+} [15–17].

On the other hand, a *N*,*O* coordination is possible when alcoholic [18] or phenolic residues are used as substituents. This, upon the deprotonation of the hydroxyl group, has led to the preparation of another series of coordination compounds, even with semimetals, including B(III) centers [19,20].

Usually, zinc and copper coordination compounds of imidazo[1,5-*a*]pyridines show remarkable luminescence properties. As an example, Volpi [21] recently reported a series of N∩N zinc complexes of 1,3-substituted imidazo[1,5-*a*]pyridines characterized by emission maxima in the blue region of the visible spectrum (410–460 nm) and with a maximum fluorescence quantum yield of 33%.

While imidazo[1,5-*a*]pyridine compounds are renowned for their luminescence properties, especially due to their usually large Stokes shifts [22], there are very few examples reporting these compounds as emissive layers in OLEDs [23], as well as in light-emitting electrochemical cells [16]. However, many of these derivatives showed high quantum yields and blue emission which, together with the aforementioned large Stokes shift, are very important properties. Moreover, it is possible to tune all these properties as well as their emission wavelength by changing the substituents on the core moiety.

On the other hand, another class of extremely well-known luminescent compounds is constituted by the boron dipyrromethene (BODIPY) derivatives. Interestingly, these species have very high quantum yields (up to 90%) and excellent chemical and photophysical stability in solution as well as in a solid state, with fluorescence lifetime in the range of 1–10 ns. A large portion of these species finds its application as a molecular sensor [24], in particular as pH indicators in organic, aqueous and mixed aqueous-organic media.

Thanks to these outstanding properties, such as high photo and chemical stability, high absorption coefficients, high quantum yields, and good solubility even in aqueous media, this family of molecules is used in the fabrication of optoelectronic devices, including OLEDs [25,26]. Unfortunately, in the solid state, BODIPY derivatives show very small Stokes shifts (5–20 nm), leading to serious self-quenching.

In our continuing research on coordination compounds with nitrogen ligands [27–30], we recently focused our attention on imidazo[1,5-*a*]pyridine scaffolds [31,32], utilized both as *N*,*N*- [33–35] or *N*,*O*- [36–39] bidentate ligands. Specifically, we combined the properties of these heterocycle and BODIPY, mimicking the latter upon the coordination of a BF_2 fragment using N∩O substituted (imidazo[1,5-*a*]pyridin-3-yl)phenolates [40,41]. These compounds showed excellent fluorescent properties and photostability and they have been used in preliminary tests as emissive materials in the fabrications of some blue emissive OLEDs [42]. Unfortunately, they displayed poor film forming properties when spin coated from a solution, thus affecting the overall performances of the devices. For these reasons, we present here a series of new developed BF_2-(imidazo[1,5-*a*]pyridin-3-yl)phenolates functionalized with long alkyl chains, in order to increase their solubility in organic solvents and their capacity to form even and homogeneous films.

2. Materials and Methods

2.1. General Remarks

Infrared Spectra were acquired on a Shimadzu Prestige-21 spectrophotometer with a 1 cm^{-1} resolution. Elemental analyses were obtained with a Perkin-Elmer CHN Analyzer 2400 Series II. NMR spectra were recorded with an AVANCE 400 Bruker spectrometer operating at 400 MHz for ^{1}H NMR and 100 MHz for $^{13}C\{^{1}H\}$ NMR. Chemical shifts are given as δ values in ppm relative to residual solvent peaks as the internal reference. *J* values are given in Hz. The UV-vis, excitation and emission spectra were measured using a fluorescence spectrometer (Edinburgh Instruments FS5) equipped with a 150 W continuous Xenon lamp as a light source and were corrected for the wavelength response

of the instrument; lifetime measurements were performed on the same FS5 Edinburgh Instruments fluorimeter equipped with an EPLED-320 (Edinburgh Instruments) as the pulsed source. Absolute fluorescence quantum yields in solution were determined using a PhotoMed GmbH K-Sphere Integrating Sphere (3.2 inch. diameter). Fluorescence quantum yields at low temperatures were estimated indirectly using the following equation:

$$\Phi_T = \Phi_{RT} \frac{I_T}{I_{RT}} \quad (1)$$

where Φ_T is the fluorescence quantum yield calculated at a given temperature, Φ_{RT} is the fluorescence quantum yield obtained experimentally at room temperature, I_T is the maximum intensity of the emission spectrum at a given temperature and I_{RT} is the maximum intensity of the emission spectrum recorded at room temperature. The correction depending on the refractive index has been neglected due to a lack of experimental data regarding the refractive indexes of dichloromethane at all the temperatures; for this reason, the calculated fluorescence quantum yields have to be intended as esteems and not as absolute values.

Analysis of the lifetime decay curve and determination of absolute quantum yields were done using Fluoracle® Software package (Version 1.9.1) which runs the FS5 instrument. **C1** and **C1-BF$_2$** have been synthesized using an already reported method [41]. All procedures have been done under inert atmosphere following the conventional Schlenk's technique. Films were obtained by spin coating on a quartz substrate 200 µL of a 5% m/m dichloromethane solution of the compound of interest and poly (methyl methacrylate) (PMMA) for one minute at a rotation speed of 5500 rpm.

2.2. General Synthesis of Pyridyl Ketones

0.5 g (20.6 mmol) of magnesium was heated under vacuum before 15 mL of anhydrous THF was added with 10 mg of iodine. The mixture was refluxed for 30 min and then a solution of 12 mmol of the 1-bromoalkane (**C3**: 1-bromopropane, **C5**: 1-bromopentane, **C10**: 1-bromodecane, **C18**:1-bromooctadecane) in 5 mL of anhydrous THF were added dropwise. The mixture was refluxed for 1 h and then cooled to room temperature. The excess of magnesium was eliminated by filtration and the resulting yellow solution was added dropwise to a solution of 10 mmol of 2-cyanopyridine in 20 mL of anhydrous THF at 0 °C. The solution was left stirring at 0 °C for 1 h and then at room temperature overnight. The solution was then quenched with 30 mL of HCl 2 M, then the pH was adjusted to 8 with an aqueous solution of NaOH 2M. The mixture was extracted with dichloromethane, washed with brine, dried over Na_2SO_4 and the solvent was removed under reduced pressure to give a brown oil which was finally purified using column chromatography (ethyl acetate:hexane 1:10) to give the final product.

2.3. General Synthesis of CX Ligands

In 30 mL of glacial acetic acid, 7.39 mmol of pyridyl ketone, 14.78 mmol of salicylaldehyde and 36.96 mmol of ammonium acetate were added. The resulting mixture was left stirring at room temperature for 7 days. The solution was then diluted with 150 mL of water and extracted with 3 × 70 mL of dichloromethane. The organic phase was washed with a saturated solution of $NaHCO_3$, dried over Na_2SO_4 and the solvent was removed under reduced pressure to give a yellow oil, which was then triturated with methanol to give the final product as a yellow solid.

C3: mp: 217°. Yield: 0.67 g (36%). Anal. Calcd (%) for $C_{16}H_{16}N_2O$: C, 76.16; H, 6.39; N, 11.10. Found (%): C, 75.86; H, 6.21; N, 11.44. ^{1}H NMR (400 MHz, $CDCl_3$, 298 K, *J* [Hz]): δ = 8.44 (t, *J* = 7.4, 1H), 7.73 (d, *J* = 7.8, 1H), 7.43 (t, *J* = 11.4, 1H), 7.31–7.21 (m, 1H), 7.14 (t, *J* = 8.6, 1H), 7.02–6.90 (m, 1H), 6.67 (m, 1H), 6.59 (t, *J* = 6.4, 1H), 2.87 (t, *J* = 7.4, 2H), 1.94–1.65 (m, 2H), 0.99 (t, *J* = 7.4, 3H). ^{13}C NMR (100 MHz, $CDCl_3$, 298 K): δ = 156.59, 134.59, 131.71, 129.50, 127.31, 123.90, 122.10, 118.95, 118.78, 117.89, 117.84, 114.58, 113.88, 28.86, 23.08, 14.08.

C5: mp: 123°. Yield: 0.73 g (35%). Anal. Calcd (%) for $C_{18}H_{20}N_2O$: C, 77.11; H, 7.19; N, 9.99. Found (%): C, 77.23; H, 7.89; N, 9.84. ^{1}H NMR (400 MHz, $CDCl_3$, 298 K, *J* [Hz]): δ = 8.42 (d, *J* = 7.3, 1H), 7.66 (d, *J* = 7.8, 1H), 7.44 (d, *J* = 9.1, 1H), 7.18 (t, *J* = 7.1, 1H), 7.14 (d, *J* = 7.5, 1H), 6.89 (t, *J* = 7.0, 1H), 6.69 (m, 1H), 6.52 (t, *J* = 7.2, 1H), 2.89 (t, *J* = 7.5, 2H), 1.80 (m, 2H), 1.42–1.30 (m, 4H), 0.90 (t, *J* = 7.0, 3H). ^{13}C NMR (100 MHz, $CDCl_3$, 298 K): δ = 156.57, 134.51, 131.81, 129.56, 127.16, 124.03, 122.14, 118.97, 118.75, 117.93, 117.83, 114.49, 113.92, 31.70, 29.49, 26.74, 22.65, 14.18.

C10: mp: 83°. Yield: 0.83 g (32%). Anal. Calcd (%) for $C_{23}H_{30}N_2O$: C, 78.82; H, 8.63; N, 7.99. Found (%): C, 79.13; H, 8.50; N, 7.67. ^{1}H NMR (400 MHz, $CDCl_3$, 298 K, *J* [Hz]): δ = 8.40 (d, *J* = 7.2, 1H), 7.73 (d, *J* = 7.7, 1H), 7.45 (d, *J* = 7.7, 1H), 7.25 (t, *J* = 7.5, 1H), 7.14 (d, *J* = 8.1, 1H), 6.96 (t, *J* = 7.5, 1H), 6.71 (m, 1H), 6.62 (t, *J* = 6.7, 1H), 2.91 (t, *J* = 7.5, 2H), 1.80 (m, 2H), 1.45–1.12 (m, 14H), 0.87 (t, *J* = 6.6, 3H). ^{13}C NMR (100 MHz, $CDCl_3$, 298 K): δ = 156.59, 134.44, 129.75, 127.17, 122.28, 119.02, 118.75, 118.12, 117.89, 114.05, 110.04, 32.05, 29.84, 29.77, 29.75, 29.62, 29.56, 29.47, 26.75, 22.85, 14.26.

C18: mp: 41°. Yield: 1.26 g (37%). Anal. Calcd (%) for $C_{31}H_{46}N_2O$: C, 80.47; H, 10.02; N, 6.05. Found (%): C, 80.01; H, 10.12; N, 5.74. ^{1}H NMR (400 MHz, $CDCl_3$, 298 K, *J* [Hz]): δ = 8.36 (d, *J* = 7.3, 1H), 7.67 (d, *J* = 7.9, 1H), 7.37 (d, *J* = 9.1, 1H), 7.22–7.16 (m, 1H), 7.06 (d, *J* = 7.9, 1H), 6.89 (t, *J* = 7.3, 1H), 6.61 (m 1H), 6.53 (t, *J* = 6.5, 1H), 2.81 (t, *J* = 7.5, 2H), 2.01–1.93 (m, 2H), 1.76–1.67 (m, 2H), 1.21 (m, 28H), 0.81 (t, *J* = 6.7 Hz, 3H). ^{13}C NMR (101 MHz, $CDCl_3$, 298 K, *J* [Hz]): δ = 156.65, 131.98, 129.51, 127.18, 123.91, 122.13, 118.94, 118.82, 117.88, 117.83, 114.60, 114.22, 113.87, 32.10, 29.88, 29.84, 29.54, 22.86, 14.26.

2.4. General Synthesis of BF_2 Compounds

2.5 mmol of **CX** was dissolved in 2 mL of dichloromethane. Then, a solution of 7.4 mmol of $BF_3{\cdot}Et_2O$ in 1 mL of dichloromethane was added dropwise. After the solution turned red, 3.6 mmol of Et_3N was added. The mixture was left stirring overnight and the resulting solid was filtered and washed with cold dichloromethane to give the final products as white solids.

C3-BF_2: mp: 194°. Yield: 0.30 g (40%). Anal. Calcd (%) for $C_{16}H_{15}N_2OBF_2$: C, 64.03; H, 5.04; N, 9.33. Found (%): C, 64.44; H, 4.88; N, 9.81. ^{1}H NMR (400 MHz, $CDCl_3$, 298 K, *J* [Hz]): δ = 8.51 (d, *J* = 6.1, 1H), 7.80 (d, *J* = 7.9, 1H), 7.57 (d, *J* = 7.5, 1H), 7.4 (t, *J* = 7.7, 1H), 7.22 (d, *J* = 8.2, 1H), 7.00 (t, *J* = 7.6, 1H), 6.97–6.84 (m, 2H), 3.14 (t, *J* = 7.6, 2H), 1.94–1.78 (m, 2H), 1.01 (t, *J* = 7.3, 3H). ^{13}C NMR (100 MHz, $CDCl_3$, 298 K): δ =155.19, 131.98, 127.71, 127.40, 122.41, 122.18, 120.76, 120.61, 119.86, 119.38, 117.26, 111.13, 26.41, 23.08, 14.15. FT-IT (ATR) (cm^{-1}): $\tilde{\nu}$ = 1034–1147 (BF_2), 2877–2980 (aliphatic C-H).

C5-BF_2: mp: 143°. Yield: 0.41 g (50%). Anal. Calcd (%) for $C_{18}H_{19}N_2OBF_2$: C, 65.88; H, 5.84; N, 8.54. Found (%): C, 65.15; H, 5.61; N, 8.66. ^{1}H NMR (400 MHz, $CDCl_3$, 298 K, *J* [Hz]): δ = 8.41 (d, *J* = 7.2 1H), 7.78 (d, *J* = 7.9, 1H), 7.62–7.48 (m, 1H), 7.32 (t, *J* = 7.6, 1H), 7.19 (d, *J* = 8.2, 1H), 7.04–6.83 (m, 3H), 3.14 (t, *J* = 7.7, 2H), 1.81 (m, 2H), 1.38 (m, 4H), 0.89 (t, *J* = 6.7, 3H). ^{13}C NMR (100 MHz, $CDCl_3$, 298 K): δ = 155.10, 131.88, 131.11, 127.61, 127.54, 122.40, 122.16, 120.74, 120.53, 119.81, 119.28, 117.25, 111.11, 31.78, 29.45, 24.47, 22.46, 14.07. FT-IT (ATR) (cm^{-1}): $\tilde{\nu}$ = 1005–1131 (BF_2), 2869–2960 (aliphatic C-H).

C10-BF_2: mp: 113°. Yield: 0.48 g (48%). Anal. Calcd (%) for $C_{23}H_{29}N_2OBF_2$: C, 69.36; H, 7.34; N, 7.03. Found (%): C, 69.20; H, 7.58; N, 6.88. ^{1}H NMR (400 MHz, $CDCl_3$, 298 K, *J* [Hz]): δ = 8.49 (d, *J* = 7.7, 1H), 7.78 (d, *J* = 7.2, 1H), 7.60 (m, 1H), 7.35 (t, *J* = 7.2, 1H), 7.27 (d, *J* = 9.4, 1H), 7.11–7.02 (m, 1H), 6.99–6.84 (m, 2H), 3.28–3.11 (m, 5H), 1.88–1.76 (m, 2H), 1.38 (m, 8H), 1.35–1.17 (m, 13H), 0.87 (t, *J* = 6.7, 3H). ^{13}C NMR (100 MHz, $CDCl_3$, 298 K): δ = 155.34, 132.15, 127.90, 127.58, 122.42, 122.17, 120.81, 120.61, 119.93, 119.54, 117.24, 111.25, 47.22, 32.03, 29.84, 29.73, 29.71, 29.47, 29.45, 24.61, 22.82, 14.25. FT-IT (ATR) (cm^{-1}): $\tilde{\nu}$ = 1012–1154 (BF_2), 2845–2949 (aliphatic C-H).

C18-BF_2: mp: 106°. Yield: 0.63 g (49%). Anal. Calcd (%) for $C_{31}H_{45}N_2OBF_2$: C, 72.93; H, 8.89; N, 5.49. Found (%): C, 72.43; H, 9.15; N, 5.11. ^{1}H NMR (400 MHz, $CDCl_3$, 298 K, *J* [Hz]): δ = 8.54 (d, *J* = 5.9, 1H), 7.83 (d, *J* = 8.0, 1H), 7.62–7.55 (m, 1H), 7.39 (t, *J* = 7.8, 1H), 7.26 (t, *J* = 6.6, 1H), 7.02 t, *J* = 7.8, 1H), 6.99–6.86 (m, 2H), 3.17 (t, *J* = 7.7, 2H),

1.83 (m, 2H), 1.48–1.16 (m, 30H), 0.89 (t, J = 6.7, 3H). ^{13}C NMR (100 MHz, $CDCl_3$, 298 K): δ = 155.27, 132.04, 131.26, 127.80, 127.56, 122.42, 122.16, 120.71, 120.64, 119.88, 119.44, 117.24, 111.17, 32.07, 29.84, 29.80, 29.74, 29.72, 29.50, 29.48, 24.59, 22.83, 14.25. FT-IT (ATR) (cm^{-1}): $\tilde{\nu}$ = 1041–1152 (BF_2), 2845–2956 (aliphatic C-H).

2.5. Computational Details

All calculations were carried out at the density functional (DFT) level of theory with the ADF2022.101 program package [43–45]. The BLYP functional plus a D3(BJ) Grimme dispersion correction energy term (BLYP-D3(BJ)) [46] was employed for all calculations. Frequency analyses were performed for all optimized structures to establish the nature of the stationary points. TD-DFT implemented in the ADF package was used to determine the excitation energies: the 20 lowest singlet-singlet excitations were calculated by using the optimized geometries. For geometry optimizations, B, C, N, O and F atoms were described through TZ2P basis sets [triple-ξ, Slater-type orbitals (STOs) plus two polarization functions]. For hydrogen atoms, the TZP basis set was employed. The corresponding augmented basis set was employed in TD-DFT calculations [47]. Restricted formalism, no-frozen-core approximation (all-electron) and no-symmetry constrains were used in all calculations. Solvent effects (CH_2Cl_2) were simulated employing the conductor-like continuum solvent model (COSMO) [48–50], as implemented in the ADF suite.

3. Results and Discussion

3.1. Syntheses and Characterization

Pyridyl ketones were prepared by following an already published method [51], by reaction between 2-cyanopyridine and the Grignard reagent derived from 1-bromoalkane. They were then used in the synthesis of the **CX** ligands through a condensation reaction with salicylaldehyde, in the presence of ammonium acetate as a source of the imidazolic nitrogen for the formation of the imidazo[1,5-*a*]pyridine ring (Scheme 1). The boron difluoride coordination compounds were obtained by reaction of $\mathbf{L^R}$ with boron trifluoride diethyl etherate, in the presence of triethylamine, in dichloromethane at room temperature (Scheme 1).

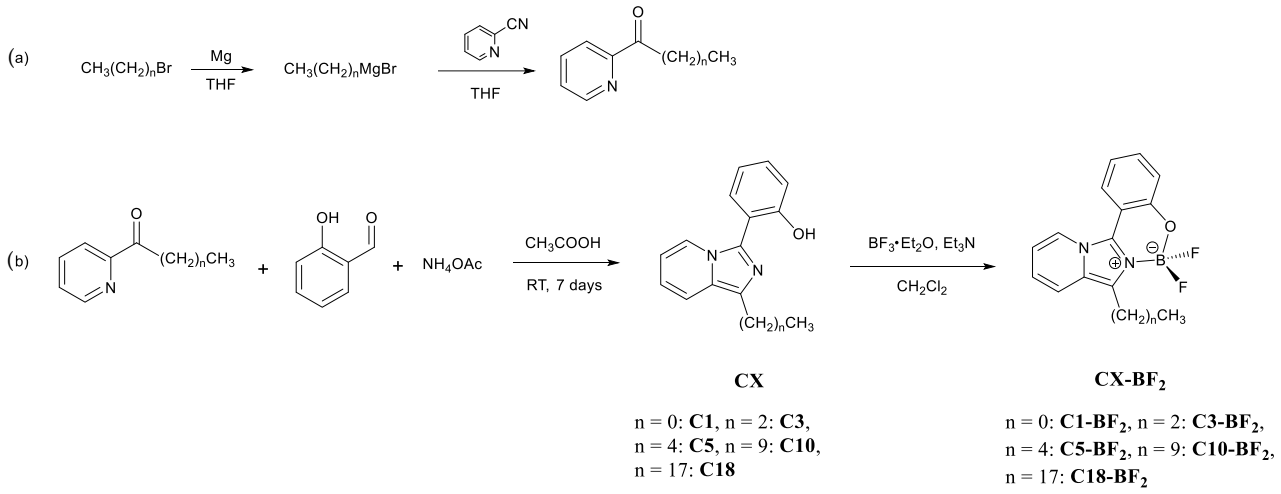

CX

n = 0: **C1**, n = 2: **C3**,
n = 4: **C5**, n = 9: **C10**,
n = 17: **C18**

CX-BF$_2$

n = 0: **C1-BF$_2$**, n = 2: **C3-BF$_2$**,
n = 4: **C5-BF$_2$**, n = 9: **C10-BF$_2$**,
n = 17: **C18-BF$_2$**

Scheme 1. Synthesis of pyridyl ketones (**a**) and **CX** and reaction with boron difluoride diethyletherate to obtain **CX-BF$_2$** (**b**).

The purity of the products was confirmed by elemental analysis and solution ^{1}H and ^{13}C{^{1}H} NMR using $CDCl_3$ as solvent.

^{1}H NMR of **CX** ligands (Figures S1–S8) displayed the aromatic signals in the range between 8.50–6.50 ppm, whereas the peaks relative to the alkylic chain could be found at 3.50–0.50 ppm. ^{13}C NMR displayed instead the resonances of the aromatic carbon atoms between 160 and 110 ppm and at about 35–14 ppm for the alkyl chain carbons (Figures S1–S8).

^{1}H NMR of **CX-BF$_2$** recorded in $CDCl_3$ (Figures S9–S16) showed the same signal pattern in a similar region.

The infrared spectrum (ATR) (Figures S17–S20) shows a series of broad signals between 1000 and 1150 cm^{-1}, in the typical range attributed to the presence of a BF_2 fragment.

3.2. Optical Properties in Solution

Ligands **CX** displayed a weak fluorescence and were not thoroughly investigated, while all the boron compounds showed blue fluorescence emission in solution (Figure 2). **C1** and **C1-BF$_2$** have been studied previously [41] and are used here as a comparison for the luminescence properties of the novel compounds.

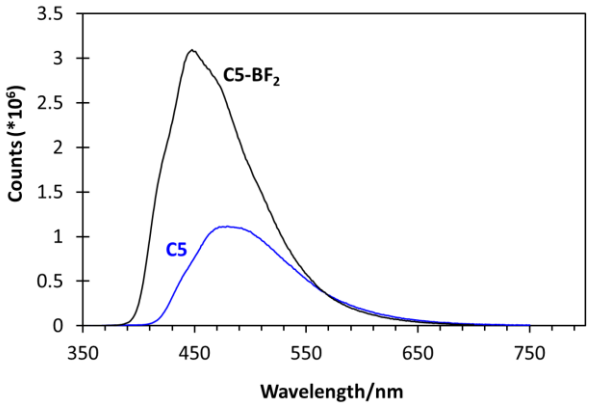

Figure 2. Comparison between the emission spectra of **C5-BF$_2$** (black trace) and **C5** (blue trace) (CH_2Cl_2, 5×10^{-5} M).

Firstly, in order to evaluate a possible solvent effect, we started the evaluation of the photophysical properties of this series of compounds from measuring the fluorescence parameters of **C3-BF$_2$**, taken as a representative example of the series, in different solvents (Table 1) (Figures S21–S23).

Table 1. Photophysical data of **C3-BF$_2$** recorded in different solvents (5×10^{-5} M).

Solvent	λ_{abs} (nm)	ε (M^{-1} cm^{-1})	λ_{em} (nm)	λ_{ex} (nm)	τ (ns)	Φ_{PL}
Dichloromethane	348	139,605	446	349	3.39	0.19
Methanol	344	115,184	442	346	3.65	0.18
Ethyl acetate	346	20,759	446	348	3.59	0.20
Toluene	351	179,357	450	351	3.68	0.19
Tetrahydrofuran	348	23,484	447	349	3.84	0.26

The absorption maxima fall in a narrow range of 5 nm, with the excitation spectra being very similar to the relative absorption spectra. The spectra recorded in toluene and ethyl acetate displayed a single absorption maximum, suppressing the peak at around 250 nm due to the strong absorption of the solvent in that region. The emission is weakly influenced as well, with a very slight bathochromic shift with decreasing the solvent polarity. Moreover, it is possible to observe the roto-vibrational structure of the band in the spectrum recorded in toluene (Figure S22). Fluorescence lifetimes are very similar, falling in the range between 3.39 and 3.84 ns. No dramatic quenching of the fluorescence was observed, thus confirming only a negligible solvent effect for this series of compounds.

Dichloromethane was then used as solvent for all the following analyses. All the photophysical data are reported in Table 2. We recorded the absorption, emission and excitation spectra of both ligands (Figure S24) and boron compounds. A net increase in the emission intensity could be observed when comparing a ligand with the respective BF_2 compound, accompanied by a slight hypsochromic shift of 20–25 nm.

Table 2. Photophysical data of **CX** and **CX-BF_2** recorded in dichloromethane solution (5×10^{-5} M).

Compound	λ_{abs} (nm)	ε (M^{-1} cm^{-1})	λ_{em} (nm)	λ_{ex} (nm)	τ (ns)	Φ_{PL}
C1	339	129,282	472	340	2.97	0.06
C1-BF_2	347	117,956	446	348	3.53	0.22
C3	337	94,620	471	340	3.04	<0.05
C3-BF_2	348	139,605	446	349	3.39	0.19
C5	339	118,515	476	341	3.05	<0.05
C5-BF_2	348	198,650	448	350	3.41	0.22
C10	338	104,460	473	339	2.86	0.05
C10-BF2	348	71,097	449	349	2.94	0.19
C18	340	193,810	477	344	2.65	0.06
C18-BF_2	348	193,189	449	348	2.95	0.20

Focusing on the boron complexes, the absorption spectra displayed two maxima, the first one at around 235 nm and the second one at 348 nm. The emission spectra are very similar among the series, with emission maxima between 446 and 449 nm (Figure 3) in the blue region, as can be observed from the CIE1931 chromaticity plot (Figure 4). The very low superposition between the emission spectra and the corresponding absorption spectra is a key feature of this class of compounds, and is fundamental in order to avoid self-absorption processes that could affect the luminescence performances. The excitation spectra largely reproduce the respective absorption traces.

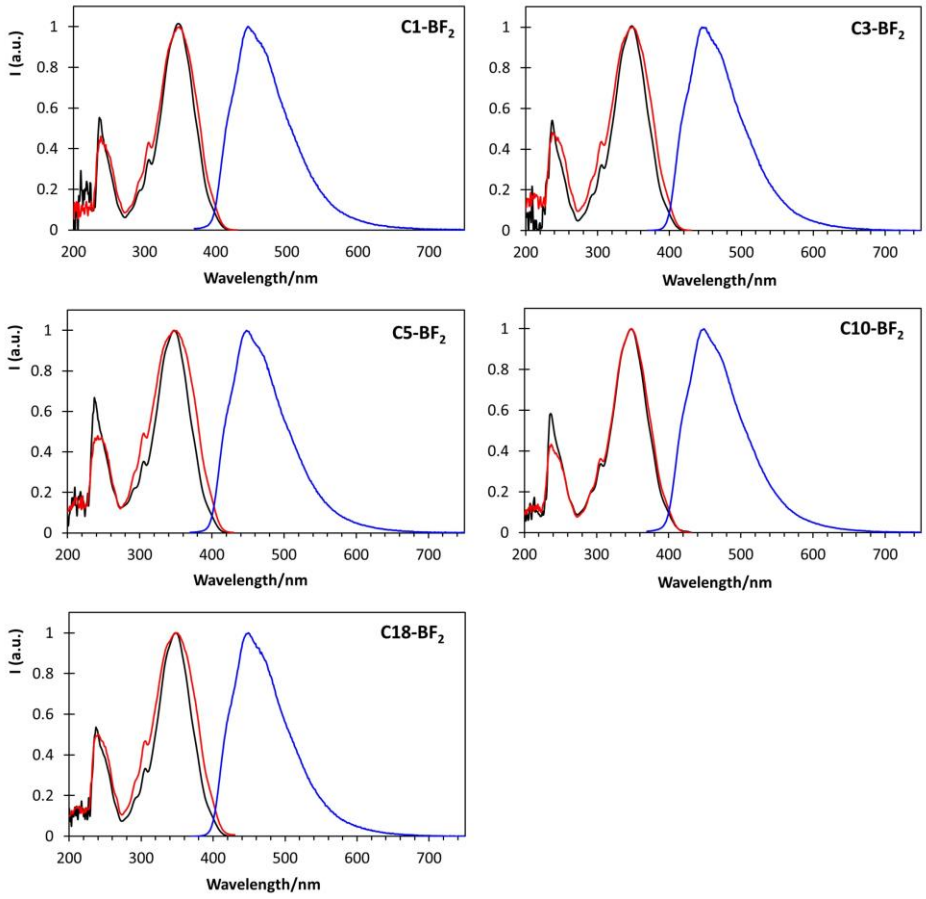

Figure 3. Absorption (black), excitation (red) and emission (blue) spectra of **CX-BF_2** compounds recorded in dichloromethane solution (5×10^{-5} M).

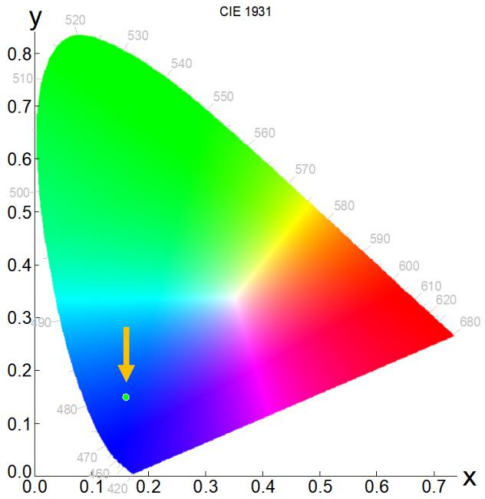

Figure 4. CIE 1931 chromaticity plot of **CX-BF$_2$** compounds recorded in dichloromethane solution (5×10^{-5} M).

All the BF_2 species displayed mono-exponential lifetime decays, in the range of 2.94 and 3.53 ns, with good fluorescence quantum yields up to 22%, with no sensible quenching effect from the alkyl chains, with the luminescence intensity not affected considerably by the presence of such groups with respect to **C1-BF$_2$**. Interestingly, even if the long chains could in principle influence the luminescence performances, they are not involved in the electronic transitions responsible for the absorption process (*vide infra*), as also corroborated by the nearly identical absorption and emission spectra throughout the series (Figure 5).

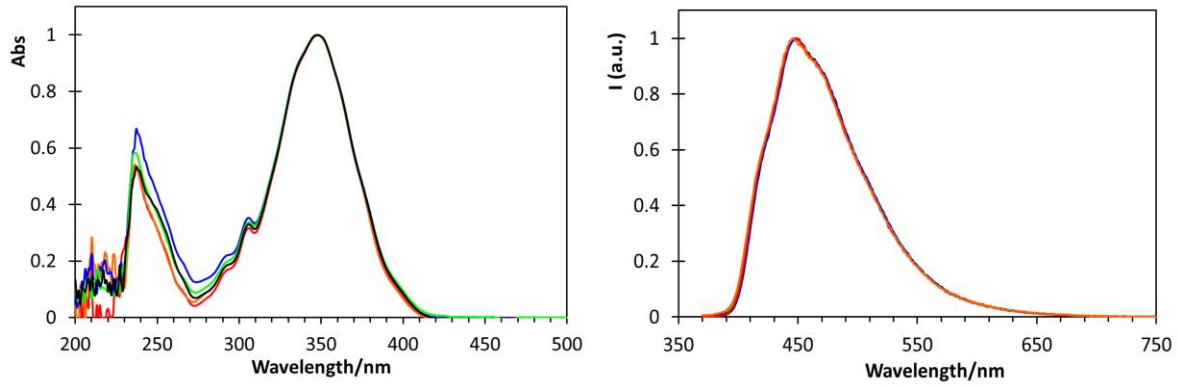

Figure 5. Normalized absorption (left) and emission (right) spectra of **CX-BF$_2$** compounds recorded in dichloromethane solution (5×10^{-5} M). **C1-BF$_2$**, orange; **C3-BF$_2$**, red; **C5-BF$_2$**, blue; **C10-BF$_2$**, green; **C18-BF$_2$**, black.

Notably, the coordination to the BF_2 fragment greatly increased the luminescent quantum yield of the ligands, reasonably by giving more rigidity to the whole system and thus preventing non-radiative decay paths given by the rotation of the phenolic ring with respect to the imidazolic portion. This is also confirmed by the orbital topology, which clearly showed no contribution from the BF_2 moiety (*vide infra*), as previously observed for **C1** and **C1-BF$_2$** [41].

Fluorescence emission analysis at lower temperatures was performed in order to establish if, by thermally preventing the vibrations of the alkyl pendants, the emission intensity could be affected. The measurements were performed in a temperature range from 0 to −80 °C: upon lowering the temperature, the luminescence intensity increased, with no shifting of the emission maxima (Figure S25). This can be better rationalized by looking at the estimated fluorescent quantum yields calculated at lower temperatures (Figure 6, Table 3).

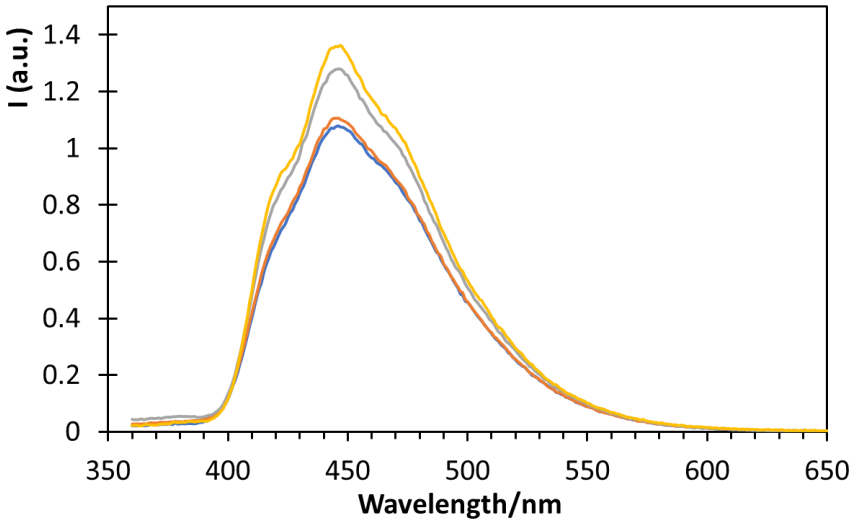

Figure 6. Emission spectra of **C5-BF$_2$** recorded in dichloromethane solution (5×10^{-5} M) at different temperatures: 298 K, blue; 273 K, orange; 233 K, grey; 193 K, yellow.

Table 3. Photoluminescence quantum yields of **CX-BF$_2$** in dichloromethane solution (5×10^{-5} M) at different temperatures. [a] experimentally recorded; [b] calculated.

L^RBF_2	298 K [a]	273 K [b]	233 K [b]	193 K [b]
C1-BF$_2$	0.22	0.22	0.31	0.30
C3-BF$_2$	0.19	0.19	0.23	0.24
C5-BF$_2$	0.22	0.23	0.26	0.28
C10-BF$_2$	0.19	0.20	0.24	0.25
C18-BF$_2$	0.20	0.22	0.25	0.24

The free ligands instead did not show an interesting increase in their emission even by lowering the temperature.

3.3. Optical Properties PMMA Films

A 5% (m/m) mixture of **CX-BF$_2$** in poly (methyl methacrylate) (PMMA) was dissolved in dichloromethane; 200 µL of the resulting solution was then spin coated on a quartz glass at a rate of 5500 rpm for 1 min. The resulting samples were used for the analysis of the fluorescence performances in thin polymeric films (Figure 7).

The fluorescence emission is still in the blue region, with a very small hypsochromic shift of less than 10 nm with respect to the emission recorded in solution. The excitation maxima are also slightly shifted towards the blue, but very close to the maxima recorded in solution. All the fluorescence lifetimes are fitted with a biexponential curve: the first lifetime is between 1.49 and 1.79 ns and the second lifetime is between 3.90 and 4.13 ns (Table 4). This could be ascribed to some interaction within the polymeric matrix, which could promote different decay pathways. This is also indirectly corroborated by the lower fluorescence quantum yields (7–14%) when compared to solution.

Interestingly, the performances of the compounds with long alkyl chains are similar to those of **C1-BF$_2$**, and can therefore be tested in the fabrication of optoelectronic devices.

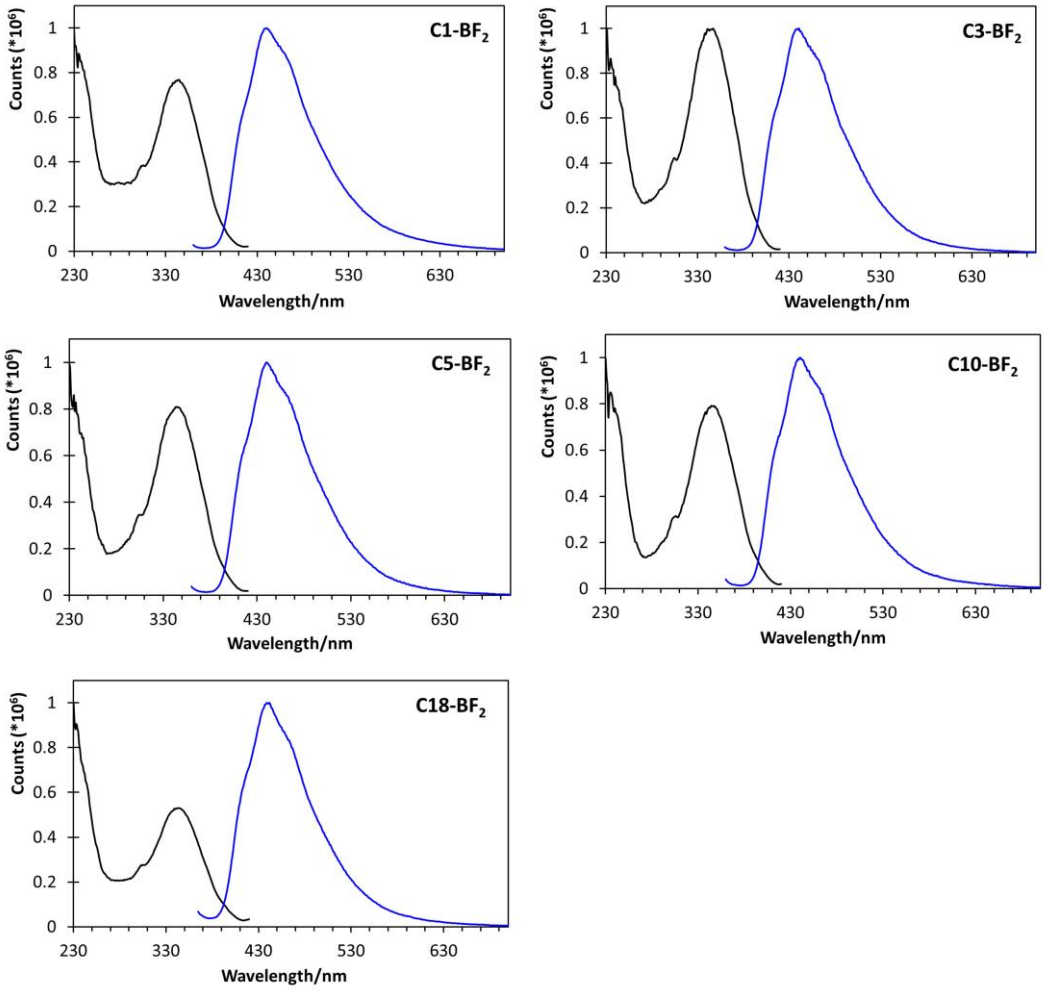

Figure 7. Excitation (black) and emission (blue) spectra of **CX-BF$_2$** compounds recorded in PMMA film.

Table 4. Photophysical data of **CX-BF$_2$** recorded in PMMA films.

Compound	λ_{em} (nm)	λ_{ex} (nm)	τ (ns)	Φ_{PL}
C1-BF$_2$	440	344	1.70 (22.8%) 4.13 (77.2%)	0.11
C3-BF$_2$	440	344	1.66 (14.0%) 3.90 (86.0%)	0.11
C5-BF$_2$	440	344	1.74 (22.0%) 4.03 (78.0%)	0.07
C10-BF$_2$	440	344	1.49 (14.0%) 3.99 (86.0%)	0.11
C18-BF$_2$	440	343	1.79 (21.8%) 4.06 (78.2%)	0.14

3.4. DFT Calculations

In analogy with the previously reported optimization of **C1-BF$_2$** from its X-ray data [41], the ground state (S_0) geometries of all other **CX-BF$_2$** compounds were optimized at the DFT level of theory. TD-DFT calculations were performed to rationalize the nature of the transitions responsible for the absorption processes.

The contributions of single orbital transitions to the absorption at lower energy are reported in Table 5. The absorption centered at about 340 nm is composed of four electronic transitions (Table 5), mainly having a HOMO-LUMO + 1 (>83.5%) character and a lower

contribution (7–8%) from HOMO-LUMO transition. The frontier molecular orbital topologies are very similar for all the compounds (Figure 8): the HOMO is delocalized over the whole molecule, whereas LUMO is mainly localized on the imidazopyridine moiety. The HOMO−1 has a strong contribution from the phenol residue, while LUMO + 1 is again distributed over the entire ligand. It is worth noting that neither the BF_2 fragment nor the alkyl chain contribute to the frontier orbitals shapes, so that they play no part in the absorption process; the BF_2 portion is giving rigidity to the system by blocking the rotation of the phenolic ring with respect to the imidazopyridine skeleton; this enhances the fluorescence properties limiting the non-radiative decay paths and indeed increasing the quantum yields of **CX-BF_2** compounds compared to the free ligands. The long alkyl chain does not affect the emission process as well; thus, it has an effect only on the physical properties of the compounds, such as solubility and film-forming. In summary, the main electronic transitions observed for **CX-BF_2** compounds can be described as intra ligand transitions (^{1}ILT), as also demonstrated by the Natural Transition Orbitals (NTOs) depicted in Figure 9 for **C5-BF_2**, taken as a representative example of the series.

Table 5. Contributions of single orbital transitions for **CX-BF_2** compounds.

	H/L + 1	H/L	H − 1/L	H − 1/L + 1
C1-BF_2	84.3%	7.7%	2.2%	1.9%
C3-BF_2	85.0%	7.7%	1.7%	1.7%
C5-BF_2	84.3%	8.1%	1.8%	1.8%
C10-BF_2	83.5%	8.2%	2.5%	1.8%
C18-BF_2	83.9%	8.3%	2.0%	1.7%

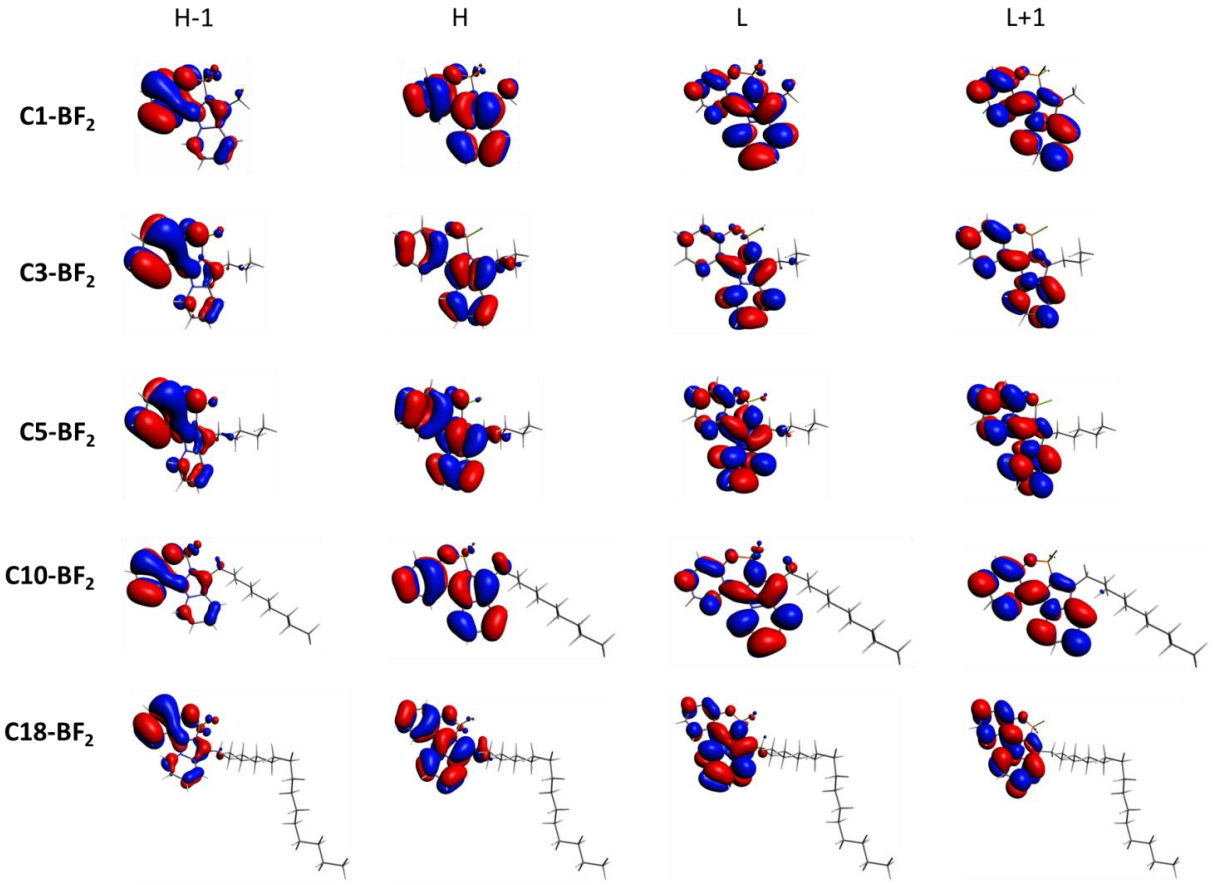

Figure 8. Frontier molecular orbitals (HOMO − 1, HOMO, LUMO, LUMO + 1) calculated for **CX-BF_2** compounds.

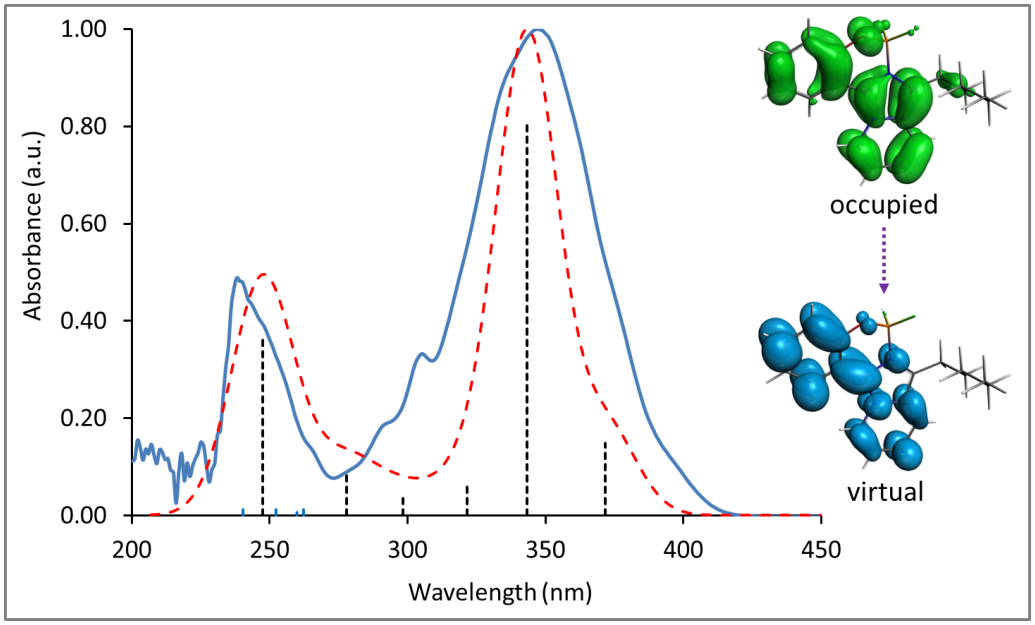

Figure 9. Calculated (dashed red line) vs. experimental (full blue line) UV-vis spectra in dichloromethane solution for compound **C5-BF$_2$**. Vertical dashed bars represent calculated transitions with oscillator strength $f > 0.1$. On the right: Natural Transition Orbitals (NTOs) calculated for compound **C5-BF$_2$**.

4. Conclusions

In this work, we presented the synthesis, characterization and study of the photophysical properties of a series of boron difluoride compounds of (imidazo[1,5-*a*]pyridine-3-yl)phenols functionalized with alkylic chains. This functionalization helped to enhance the solubility and film formation properties of these compounds, with little to no alteration to their luminescence performances. Nevertheless, all these compounds displayed a blue fluorescence emission, with large Stokes shifts and good absolute quantum yields, thus paving the way for their use as emissive materials in blue emissive optoelectronic devices. In particular, they will be tested in the fabrication of blue organic light emitting diodes (OLEDs), continuing a preliminary study where **C1-BF$_2$** was already successfully tested. Moreover, the almost complete inertness of the luminescence performances towards the substitution could be further exploited functionalizing these compounds with several other substituents.

Supplementary Materials: The following supporting information can be downloaded at: https://www.mdpi.com/article/10.3390/colorants2020012/s1, Figures S1–S16: Full ^{1}H, ^{13}C NMR spectra of **CX** and **CX-BF$_2$** compounds; Figures S17–S20: Infrared (ATR) spectra; Figures S21–S25: Absorption, excitation and emission spectra for **CX** and **CX-BF$_2$** compounds.

Author Contributions: Conceptualization, G.C., S.B. and G.A.A.; Methodology, G.C. and S.B.; Software, G.A.A.; Investigation, G.C. and A.C.; Writing—Original Draft Preparation, G.C.; Writing—Review and Editing, G.C., A.C., S.B. and G.A.A.; Supervision, S.B. and G.A.A.; Funding Acquisition, A.C., S.B. and G.A.A. All authors have read and agreed to the published version of the manuscript.

Funding: This research was partially funded by Ministero dell'Università e della Ricerca (D.M. 351, 9/4/2022), University of Insubria (FAR2022), Fondazione Banca del Monte di Lombardia (FBML-2013).

Institutional Review Board Statement: Not applicable.

Informed Consent Statement: Not applicable.

Data Availability Statement: No additional data were created.

Acknowledgments: The authors thank the Ministero dell'Università e della Ricerca (MUR) and the University of Insubria for partial financial support. Fondazione Banca del Monte di Lombardia (FBML) is warmly acknowledged for generous funding through the Research Project *"Transiton-metals based coordination compounds for light emitting device applications"*. This paper and related research have been conducted while attending (AC) the PhD programme in PhD in Sustainable Development And Climate Change at the University School for Advanced Studies IUSS Pavia, Cycle XXXVIII (URL: www.phd-sdc.it (accessed on 31 March 2023)).

Conflicts of Interest: The authors declare no conflict of interest.

References

1. Volpi, G. Luminescent Imidazo[1,5-*a*]pyridine Scaffold: Synthetic Heterocyclization Strategies-Overview and Promising Applications. *Asian J. Org. Chem.* **2022**, *11*, e202200171.
2. Volpi, G.; Rabezzana, R. Imidazo[1,5-*a*]pyridine derivatives: Useful, luminescent and versatile scaffolds for different applications. *New J. Chem.* **2021**, *45*, 5737–5743. [CrossRef]
3. Kamal, A.; Ramakrishna, G.; Janaki Ramaiah, M.; Viswanath, A.; Subba Rao, A.V.; Bagul, C.; Mukhopadyay, D.; Pushpavalli, S.N.C.V.L.; Pal-Bhadra, M. Design, synthesis and biological evaluation of imidazo[1,5-*a*]pyridine-PBD conjugates as potential DNA-directed alkylating agents. *Med. Chem. Commun.* **2013**, *4*, 697.
4. Kamal, A.; Rao, A.V.S.; Nayak, V.L.; Reddy, N.V.S.; Swapna, K.; Ramakrishna, G.; Alvala, M. Synthesis and biological evaluation of imidazo[1,5-*a*]pyridine-benzimidazole hybrids as inhibitors of both tubulin polymerization and PI3K/Akt pathway. *Org. Biomol. Chem.* **2014**, *12*, 9864–9880. [CrossRef]
5. Khan, M.S.; Baig, M.H.; Ahmad, S.; Ahmad Siddiqui, S.; Srivastava, A.K.; Srinivasan, K.V.; Ansari, I.A. Design, Synthesis, Evaluation and Thermodynamics of 1-Substituted Pyrirylimidazo[1,5-*a*]Pyridine Derivates as Cysteine Protease Inhibitors. *PLoS ONE* **2013**, *8*, 69982.
6. Ge, Y.Q.; Li, F.R.; Zhang, Y.J.; Bi, Y.S.; Cao, X.Q.; Duan, G.Y.; Wang, J.W.; Liu, Z.L. Synthesis, crystal structure, optical properties and antibacterial evaluation of novel imidazo[1,5-*a*]pyridine derivatives bearing a hydrazone moiety. *Luminescence* **2013**, *29*, 293–300. [CrossRef]
7. Nirogi, R.; Mohammed, A.R.; Shinde, A.K.; Bogaraju, N.; Gagginapalli, S.R.; Ravella, S.R.; Kota, L.; Bhyra-puneni, G.; Muddana, N.R.; Benade, V.; et al. Synthesis and SAR of Imidazo[1,5-*a*]pyridine derivatives as 5-HT4 receptor partial agonists for the treatment of cognitive disorders associated with Alzheimer's disease. *Eur. J. Med. Chem.* **2015**, *103*, 289.
8. Ge, Y.; Xing, X.; Liu, A.; Ji, R.; Shen, S.; Cao, X. A novel imidazo[1,5-*a*]pyridine-rhodamine FRET system as an efficient ratiometric fluorescent probe for Hg^{2+} in living cells. *Dye. Pigment.* **2017**, *146*, 136–142. [CrossRef]
9. Chen, S.; Li, H.; Hou, P. A novel imidazo[1,5-*a*]pyridine-based fluorescent probe with a large Stokes shift for imaging hydrogen sulfide. *Sens. Actuators B* **2018**, *256*, 1086.
10. Chen, S.; Hou, P.; Sun, J.; Wang, H.; Liu, L. Imidazo[1,5-α]pyridine-based fluorescent probe with a large Stokes shift for specific recognition of sulfite. *Spectrochim. Acta Part A Mol. Biomol. Spectrosc.* **2020**, *225*, 117508. [CrossRef]
11. Zhang, X.; Huang, Y.; Zhang, Q.; Li, D.; Li, Y. A One-Dimensional Cadmium Coordination Polymer: Synthesis, Structure, and Application as Luminescent Sensor for Cu^{2+} and $CrO_4^{2-}/Cr_2O_7^{2-}$ Ions. *Eur. J. Inorg. Chem.* **2021**, *14*, 1349. [CrossRef]
12. Priyanga, S.; Khamrang, T.; Velusamy, M.; Karthi, S.; Ashokkumar, B.; Mayilmurugan, R. Coordination geometry-induced optical imaging of L-cysteine in cancer cells using imidazopyridine-based copper(II) complexes. *Dalton Trans.* **2019**, *48*, 1489. [PubMed]
13. Hoshi, K.; Itaya, M.; Tahara, K.; Matsumoto, A.; Tabata, A.; Nagamune, H.; Yoshida, Y.; Hase, E.; Minamikawa, T.; Yasui, T.; et al. Two-photon excitable boron complex based on tridentate imidazo[1,5-*a*]pyridine ligand for heavy-atom-free mitochondria-targeted photodynamic thera-py. *RSC Adv.* **2021**, *11*, 26403.
14. Volpi, G.; Garino, C.; Priola, E.; Diana, E.; Gobetto, R.; Buscaino, R.; Viscardi, G.; Barolo, C. Facile syntesis of novel blue light and large Stokes shift emitting tetradentate polyazines based on imidazo[1,5-*a*]pyridine–Part 2. *Dye. Pigment.* **2017**, *143*, 284.
15. Álvarez, C.M.; Álvarez-Miguel, L.; García-Rodríguez, R.; Miguel, D. Complexes with 3-(pyridin-2-yl)imidazo[1,5-*a*]pyridine ligands by spontaneous dimerization of pyridine-2-carboxaldehyde within the coordination sphere of manganese(ii) in a one-pot reaction. *Dalton Trans.* **2012**, *41*, 7041–7046. [CrossRef] [PubMed]
16. Fresta, E.; Volpi, G.; Garino, C.; Barolo, C.; Costa, R.D. Contextualizing yellow light-emitting electrochemical cells based on a blue-emitting imidazo-pyridine emitter. *Polyhedron* **2018**, *140*, 129–137. [CrossRef]
17. Guckian, A.L.; Doering, M.; Ciesielski, M.; Walter, O.; Hjelm, J.; O'Boyle, N.M.; Henry, W.; Browne, W.R.; McGarvey, J.J.; Vos, J.G. Assessment of intercomponent interaction in phenylene bridged dinuclear ruthenium(ii) and osmium(ii) polypyridyl complexes. *Dalton Trans.* **2004**, *33*, 3943–3949. [CrossRef]
18. Murai, T.; Nagaya, E.; Miyahara, K.; Shibahara, F.; Maruyama, T. Synthesis and Characterization of Boron Complexes of Imidazo[1,5-*a*]pyridylalkyl Alcohols. *Chem. Lett.* **2013**, *42*, 828–830. [CrossRef]
19. Yagishita, F.; Kinouchi, T.; Hoshi, K.; Tezuka, Y.; Jibu, Y.; Karatsu, T.; Uemura, N.; Yoshida, Y.; Mino, T.; Sakamoto, M.; et al. Highly efficient blue emission from boron complexes of 1-(o-hydroxyphenyl)imidazo[1,5-*a*]pyridine. *Tetrahedron* **2018**, *74*, 3728–3733. [CrossRef]

20. Yagishita, F.; Hoshi, K.; Mukai, S.; Kinouchi, T.; Katayama, T.; Yoshida, Y.; Minagawa, K.; Furube, A.; Imada, Y. Effect of Phenolic Substituent Position in Boron Complexes of Imidazo[1,5-*a*]pyridine. *Asian J. Org. Chem.* **2022**, *11*, e202200040. [CrossRef]
21. Volpi, G.; Priola, E.; Garino, C.; Daolio, A.; Rabezzana, R.; Benzi, P.; Giordana, A.; Diana, E.; Gobetto, R. Blue fluorescent zinc(II) complexes based on tunable imidazo[1,5-*a*]pyridines. *Inorganica Chim. Acta* **2020**, *509*, 119662. [CrossRef]
22. Volpi, G.; Magnano, G.; Benesperi, I.; Saccone, D.; Priola, E.; Gianotti, V.; Milanesio, M.; Conterosito, E.; Barolo, C.; Viscardi, G. One pot synthesis of low-cost emitters with large Stokes' shift. *Dye. Pigment.* **2017**, *137*, 152–164. [CrossRef]
23. Nakatsuka, M.; Shimamura, T.K. Organic electroluminescent element. *Chem. Abstr.* **2001**, *134*, 170632.
24. Boens, N.; Leen, V.; Dehaen, W. Fluorescent indicators based on BODIPY. *Chem. Soc. Rev.* **2012**, *41*, 1130.
25. Squeo, B.M.; Pasini, M. BODIPY platform: A tunable tool for green to NIR OLEDs. *Supramol. Chem.* **2020**, *32*, 56–70. [CrossRef]
26. Brom, J.M., Jr.; Langer, J.L. Electroluminescence from pyrromethene dyes in doped polymer hosts. *Alloys Compd.* **2002**, *1*, 112.
27. Ardizzoia, G.A.; Brenna, S.; Therrien, S. The Adaptable Coordination Chemistry of 6-Chloro-2-(quinolin-2-yl)-2,4-dihydro-1H-benzo[d][1,3]oxazine Towards Zinc(II) and Mercury(II). *Eur. J. Inorg. Chem.* **2010**, *21*, 3365.
28. Ardizzoia, G.A.; Brenna, S.; Durini, S.; Therrien, B.; Trentin, I. The Goldilocks principle in action: Synthesis and structural characterization of a novel {Cu4(μ3-OH)4} cubane stabilized by monodentate ligands. *Dalton Trans.* **2013**, *42*, 12265.
29. Ardizzoia, G.A.; Bea, M.; Brenna, S.; Therrien, B. A Quantitative Description of the σ-Donor and π-acceptor Properties of Substituted Phenanthrolines. *Eur. J. Inorg. Chem.* **2016**, *23*, 3829.
30. Ardizzoia, G.A.; Brenna, S.; Civati, F.; Colombo, V.; Sironi, A. A phosphorescent copper(i) coordination polymer with sodium 3,5-dimethyl-4-sulfonate pyrazolate. *Crystengcomm* **2017**, *19*, 6020–6027. [CrossRef]
31. Marchesi, A.; Brenna, S.; Ardizzoia, G.A. Synthesis and emissive properties of a series of tetrahydro (imidazo[1,5-*a*]pyrid-3-yl)phenols: A new class of large Stokes shift organic dyes. *Dye. Pigment.* **2018**, *161*, 457–463. [CrossRef]
32. Colombo, G.; Ardizzoia, G.A.; Brenna, S. Imidazo[1,5-*a*]pyridine-based derivatives as highly fluorescent dyes. *Inorganica Chim. Acta* **2022**, *535*, 120849. [CrossRef]
33. Ardizzoia, G.A.; Brenna, S.; Durini, S.; Therrien, B.; Veronelli, M. Synthesis, Structure, and Photphysical Properties of Blue-Emitting Zinv(II) Complexes with 3-aryl-Substituted 1-Pyridylimidazo[1,5-*a*]pyridine Ligands. *Eur. J. Inorg. Chem.* **2014**, *26*, 4310. [CrossRef]
34. Ardizzoia, G.A.; Brenna, S.; Durini, S.; Therrien, B. Synthesis and characterization of luminescent zinc(II) complexes with a N,N-bidentate 1-pyridylimidazo[1,5-*a*]pyridine ligand. *Polyhedron* **2015**, *90*, 214–220. [CrossRef]
35. Durini, S.; Ardizzoia, G.A.; Therrien, B.; Brenna, S. Tuning the fluorescence emission in mononuclear heteroleptic trigonal silver(i) complexes. *New J. Chem.* **2017**, *41*, 3006–3014. [CrossRef]
36. Ardizzoia, G.A.; Ghiotti, D.; Therrien, B.; Brenna, S. Homoleptic complexes of divalent metals bearing N,O-bidentate imidazo[1,5-*a*]pyridine ligands: Synthesis, X-ray characterization and catalytic activity in the Heck reaction. *Inorganica Chim. Acta* **2018**, *471*, 384–390. [CrossRef]
37. Ardizzoia, G.A.; Colombo, G.; Therrien, B.; Brenna, S. Tuning the Fluorescence Emission and HOMO-LUMO Band Gap in Homoleptic Zinc(II) Complexes with N,O-Bidentate (Imidazo[1,5-*a*]pyrid-3-yl)phenols. *Eur. J. Inorg. Chem.* **2019**, *13*, 1825. [CrossRef]
38. Strianese, M.; Brenna, S.; Ardizzoia, G.A.; Guarnieri, D.; Lamberti, M.; D'Auria, I.; Pellecchia, C. Imidazo-pyridine-based zinc(ii) complexes as fluorescent hydrogen sulfide probes. *Dalton Trans.* **2021**, *50*, 17075–17085. [CrossRef]
39. D'Alterio, M.C.; D'Auria, I.; Gaeta, L.; Tedesco, C.; Brenna, S.; Pellecchia, C. Are Well Performing Catalysts for the Ring Opening Polymerization of l-Lactide under Mild Laboratory Conditions Suitable for the Industrial Process? The Case of New Highly Active Zn(II) Catalysts. *Macromolecules* **2022**, *55*, 5115–5122. [CrossRef]
40. Colombo, G.; Romeo, A.; Ardizzoia, G.A.; Furrer, J.; Therrien, B.; Brenna, S. Boron difluoride functionalized (tetrahydroimidazo [1,5-*a*]pyridine-3-yl)phenols: Highly fluorescent blue emissive materials. *Dye. Pigment.* **2020**, *182*, 108636. [CrossRef]
41. Colombo, G.; Ardizzoia, G.A.; Furrer, J.; Therrien, B.; Brenna, S. Driving the Emission Towards Blue by Controlling the HOMO-LUMO Energy Gap in BF2-Functionalized 2-(Imidazo[1,5-*a*]pyridine-3-yl)phenols. *Chem. Eur. J.* **2021**, *27*, 12380. [CrossRef] [PubMed]
42. Colombo, G. Blue Emissive Materials for Optoelectronic Devices. Ph.D. Thesis, Università degli Studi dell'Insubria, Como, Italy, April 2022.
43. Te Velde, G.; Bickelhaupt, F.M.; Fonseca Guerra, C.; van Gisbergen, S.J.A.; Snijders, J.G.; Ziegler, T. Chemistry with ADF. *J. Comput. Chem.* **2001**, *22*, 931. [CrossRef]
44. Fonseca Guerra, C.; Snijders, J.G.; Te Velde, G.; Baerends, E.J. Towards an order-N- DFT method. *Theor. Chem. Acc.* **1998**, *99*, 391. [CrossRef]
45. Baerends, E.J.; Ziegler, T.; Autschbach, J.; Bashford, D.; Bérces, A.; Bickelhaupt, F.M.; Bo, C.; Boerrigter, P.M.; Cavallo, L.; Chong, D.P.; et al. *ADF2014, SCM, Theoretical Chemistry*; Vrije Universiteit: Amsterdam, The Netherlands. Available online: http://www.scm.com (accessed on 31 March 2023).
46. Grimme, S.; Ehrlich, S.; Goerigk, L. Effect of the damping function in dispersion corrected density functional theory. *J. Comput. Chem.* **2011**, *32*, 1456. [CrossRef] [PubMed]
47. Chong, D.P. Augmenting basis set for time-dependent density functional theory calculation of excitation energies: Slater-type orbitals for hydrogen to krypton. *Mol. Phys.* **2005**, *103*, 749. [CrossRef]

48. Klamt, A.; Schürmann, G.J. COSMO: A new approach to dielectric screening in solvents with explicit expressions for the screening energy and its gradient. *J. Chem. Phys.* **1993**, *2*, 799. [CrossRef]
49. Klamt, A.; Jonas, V. Treatment of the outlying charge in continuum solvation models. *J. Chem. Phys.* **1996**, *105*, 9972. [CrossRef]
50. Pye, C.C.; Ziegler, T. An implementation of the conductor-like screening model of solvation within the Amsterdam density functional package. *Theor. Chem. Acc.* **1999**, *101*, 396. [CrossRef]
51. Wu, Q.; Han, S.; Ren, X.; Lu, H.; Li, J.; Zou, D.; Wu, Y.; Wu, Y. Pd-Catalyzed Alkylation of (Iso)quinolines and Arenes: 2-acylpyridine Compounds as Alkylation Reagents. *Org. Lett.* **2018**, *20*, 6345–6348. [CrossRef]